Mitochondrial and Microsomal Ferric b_5 Cytochromes Exhibit Divergent Conformational Plasticity in the Context of a Common Fold†

Mario Simeonov,‡ Adriana Altuve,‡ Michael A. Massiah,§ An Wang,‡ Margaret A. Eastman,|| David R. Benson,‡ and Mario Rivera*,‡

Department of Chemistry, The University of Kansas, 1251 Wescoe Hall Drive, Lawrence, Kansas 66045-7582, Department of Biochemistry and Molecular Biology, Oklahoma State University, Stillwater, Oklahoma 74078, and Department of Chemistry, Oklahoma State University, Stillwater, Oklahoma 74078

Received March 28, 2005; Revised Manuscript Received May 10, 2005

ABSTRACT: Native-state hydrogen−deuterium exchange (HDX) monitored by NMR spectroscopy has been used to compare conformational plasticity in ferric rat liver outer mitochondrial membrane cytochrome b_5 (rOM b_5) and ferric bovine liver microsomal cytochrome b_5 (bMc b_5). Analysis of the data indicated that rOM b_5 is the less conformationally flexible protein on the time scale probed by the HDX experiments. The data also suggest a likely contributor to the much higher kinetic barrier for the release of hemin from OM b_5s in comparison to Mc b_5s, a characteristic that may be to a large extent the source of their divergent functional properties. Specifically, the data indicate that conformational mobility within helices α4 and α5, which flank the loop harboring axial ligand His63, is considerably more restricted in rOM b_5 than in bMc b_5. The lower conformational flexibility of α4 and α5 in rOM b_5 can reasonably be attributed to more extensive hydrophobic packing in that region of the protein, arising from two conserved side chain packing motifs in OM cytochrome b_5s [Altuve, A., Wang, L., Benson, D. R., and Rivera, M. (2004) *Biochem. Biophys. Res. Commun. 314,* 602−609].

Mammals possess two genes encoding membrane-associated isoforms of cytochrome b_5, which likely arose via duplication of a primordial gene and subsequent functional divergence. One gene encodes an isoform of 134 residues (*1*−*3*) that is tail-anchored to the membrane of the endoplasmic reticulum (microsomal, or Mc b_5), where it donates electrons to fatty acid desaturases, cytochrome P450s, and other redox partners (*4*−*6*). The second b_5 gene encodes a 146-residue protein that is tail-anchored to the outer mitochondrial membrane (OM b_5) (*7*, *8*). Mc b_5s identified from a variety of mammals exhibit a high degree of amino acid sequence homology (*9*), and it is therefore not surprising that studies of select proteins have revealed broadly similar biophysical properties. OM b_5s are comparatively less well-known than Mc b_5s, having been positively identified in only three organisms to date (rats, mice, and humans) (*10*). Studies in our laboratories with recombinant proteins representing the soluble heme-binding domains of rat OM (rOM) and human OM b_5 have indicated that biophysical properties of OM b_5s from different organisms are also broadly similar, but markedly different from those of their Mc counterparts (*10*). For example, reduction potentials of rat OM b_5 and human OM b_5 are significantly more negative (*10*−*13*) than those of Mc b_5s.

OM b_5s are also considerably more stable than Mc b_5s toward thermal and chemical denaturation, a property that has been traced partially to a higher kinetic barrier for dissociation of hemin[1] (ferric heme) (*9*, *10*, *14*). This is manifested in much slower rates of equilibration of the two hemin orientational isomers that are formed in equimolar amounts upon initial binding of the prosthetic group by the polypeptide. Equilibration to the thermodynamically dictated ratio involves rotation of the heme about the $\alpha-\gamma$ meso axis (*15*). In the case of the Mc b_5s, conversion of the less stable isomer to the more stable isomer occurs at measurable rates even at 25 °C (pH 7) (*15*−*19*). The corresponding reaction at 37 °C is complete within a few hours. In comparison, equilibration of hemin orientational isomers in OM b_5s proceeds at discernible rates only if the temperature is above ∼50 °C. At physiologically relevant temperatures, hemin in OM b_5s is kinetically trapped (*9*, *20*). The differences in biophysical properties of OM and Mc b_5s noted above, almost certainly related to their specialized subcellular roles, are encoded in their amino acid sequences. Indeed, Mc and OM b_5s, both within and between species, exhibit a lower degree of amino acid sequence homology than either individual isoform does. The full-length forms of rat OM (rOM) and bovine Mc (bMc) b_5, the two proteins studied in our laboratories, are 49% identical and 68% similar. The level of homology is somewhat greater (63% identical and 82%

† This work was supported by grants from the National Science Foundation (MCB-0446326) and the National Institutes of Health (GM-50503).

* To whom correspondence should be addressed. Phone: (785) 864-4936. Fax: (785) 864-5396. E-mail: mrivera@ku.edu.

‡ The University of Kansas.

§ Department of Biochemistry and Molecular Biology, Oklahoma State University.

|| Department of Chemistry, Oklahoma State University.

[1] Abbreviations: hemin, iron(III) protoporphyrin IX; rOM b_5, ferric rat liver outer mitochondrial membrane cytochrome b_5; bMc b_5, ferric bovine liver microsomal cytochrome b_5; HDX, hydrogen−deuterium exchange; NMR, nuclear magnetic resonance; MD, molecular dynamics simulations; IPTG, isopropyl thiogalactose; CSI, chemical shift index.

10.1021/bi050564l CCC: $30.25
Published on Web 06/04/2005

```
                -1 1          11         21         31
bMc b5            AVKYYTLE EIQKHNNSKS TWLILHYKVY DLTKFLEEHP
rOM b5    NGQGS DPAVTYYRLE EVAKRNTAEE TWMVIHGRVY DITRFLSEHP
                                     *       *       *   *

          41         51         61         71         81
bMc b5     GGEEVLREQA GGDATENFED VGHSTDAREL SKTFIIGELH PDDR
rOM b5     GGEEVLLEQA GADATESFED VGHSPDAREM LKQYYIGDVH PNDLKPK
                    *                       *
```

FIGURE 1: Amino acid sequences of the recombinant bMc and rOM b_5 polypeptides used in this study (63% identical and 82% similar based on residues 3−84). The numbering is based on the scheme introduced by Mathews for the lipase fragment of bovine Mc b_5 (*51*). The asterisks below the rOM b_5 sequence denote the positions of residues participating in the conserved rOM b_5 hydrophobic patches (see the text for details).

similar) when only the soluble heme-binding domains are considered (see Figure 1).

The first proposed role for OM b_5, the reduction of ascorbate radical in liver (*21*), is supported by experimental evidence (*11*) indicating sufficient driving force to sustain the reaction. This is not the case for Mc b_5 because of its more positive reduction potential. More recently, two research groups independently reported that OM b_5 modulates sex hormone synthesis by cytochrome $P450_{17}\alpha$ in testis (*22*, *23*), and in fact, OM b_5 is the only isoform expressed in that tissue (*22*). Mc b_5s perform this role less efficiently, perhaps again in part because they have a higher reduction potential and therefore a weaker driving force for electron delivery (*18*, *24*, *25*). An additional possibility is that electron transfer from b_5 to $P450_{17}\alpha$ requires conformational changes that are triggered more efficiently by the binding of OM b_5 than of Mc b_5. This strongly suggests potentially different requirements for specificity in protein−protein recognition by the two isoforms. In fact, the importance of protein dynamics in modulating function is now well-established (*26*−*28*). In this context, it has been proposed that the ability of Mc b_5s to recognize their multiple redox protein partners requires significant adaptability (*29*). Results of molecular dynamics (MD) simulations (*29*) were used to suggest that Mc b_5s achieve this adaptability via conformational mobility (plasticity) of structural motifs at the protein surface. However, these authors noted that high conformational flexibility can also compromise stability by facilitating release of hemin. It is therefore very interesting that (1) rOM b_5 exhibits much lower surface plasticity than bMc b_5 does in MD simulations (*9*, *30*) and (2) dissociation of hemin from rOM b_5 is accompanied by a much smaller increase in polypeptide size and dynamic mobility than is release of hemin from bMc b_5 (*31*). The much higher kinetic barrier for release of hemin from OM b_5s than from Mc b_5s (*9*, *10*, *14*), as well as its more favorable interactions with $P450_{17}\alpha$, may therefore be an indication that OM b_5s have fewer protein redox partners and therefore were subjected to less pressure to evolve conformational plasticity.

Despite the fact that Mc and OM b_5s exhibit such divergent biophysical (*9*−*11*, *14*, *20*, *31*), dynamic, and functional (*21*−*23*) properties, the two isoforms adopt almost identical folds as demonstrated by X-ray crystallographic studies of Mc b_5 (*32*) and rOM b_5 (*33*). Previous studies in our laboratories aimed at probing the structural basis for the divergent OM and Mc b_5 properties led to identification of two conserved hydrophobic networks in the OM proteins (see Figure 1) (*9*, *10*, *14*). The observation in MD simulations of lower polypeptide conformational mobility in rOM b_5 than in bMc b_5 provided support to a hypothesis that the conserved hydrophobic networks make a key contribution to the higher kinetic barrier for release of hemin from the OM protein. However, MD simulations provide information about a very short time scale, 1 ns in this case, preventing us from confirming this hypothesis. It is possible that additional differences in conformational flexibility taking place over longer time scales are even more important in differentiating the functional and stability properties of OM and Mc b_5s.

We have also replaced the amino acids contributing to the hydrophobic networks in rOM b_5 with the corresponding residues characteristic of Mc b_5s, which form less extensive hydrophobic packing interactions (*9*, *14*). Complete replacement yielded a crystallographically characterized rOM b_5 quintuple mutant (essentially an rOM−bMc b_5 "hybrid") with stability properties similar to those of bMc b_5, and with an enhanced propensity to release hemin to apomyoglobin (apoMb) (*14*). While this further supports a key role for the conserved OM b_5 hydrophobic patches in raising its hemin release barrier relative to that of Mc b_5, it does not provide detailed information about polypeptide dynamics. In addition, we found that the rOM−bMc b_5 hybrid releases hemin to apoMb much more slowly than does wild-type bMc b_5 under physiologically relevant conditions (*14*). This indicates that the relationship between the OM b_5 hydrophobic patches and stability is much more complex than originally thought.

A complete understanding of the differences in OM and Mc b_5 polypeptide dynamics is desirable given the strong possibility that they are important for function. Such an understanding requires global information acquired over a time scale that is longer than that which can be achieved in MD simulations, and at a level of structural resolution that is not available via study of hybrid mutants. The work reported herein describes the initial stages of our efforts in obtaining that information. We began with the premise that release of hemin from a given b_5 correlates with the extent of conformational mobility asssociated with the polypeptide defining its heme-binding pocket. To test this hypothesis, we carried out native-state amide hydrogen−deuterium exchange (HDX) experiments with rOM and bMc b_5 monitored by NMR spectroscopy. Results and insights obtained from these experiments are reported herein.

EXPERIMENTAL PROCEDURES

Sample Preparation. ^{13}C- and ^{15}N-labeled b_5 cytochromes were expressed using recombinant pET11a plasmids harboring synthetic genes encoding the water soluble domain of rat OM b_5 (residues M−6 to K87) (*34*) and bovine Mc b_5 (residues M2 to R84) (*14*, *35*). Each of the plasmids was transformed into *Escherichia coli* BL21(DE3), and the cells

were grown in 1 L of M9 minimal medium (*36*) at 37 °C and shaken at 220 rpm until the optical density of the cell culture at 600 nm (OD_{600}) reached 0.7. Each 1 L culture was pelleted by centrifugation, the supernatant discarded, and the pellet washed with fresh M9 medium not containing glucose and trace metals. The resultant suspension was centrifuged again and the supernatant discarded. In protein expressions aimed at preparing OM b_5 for its use in resonance assignments, each pellet was resuspended in 1 L of M9 medium containing 2 g of [$^{13}C_6$]-D-glucose and 1 g of $^{15}NH_4Cl$ (Cambridge Isotope Laboratories Inc.). In expressions aimed at preparing OM or Mc b_5 for use in HDX experiments, each pellet was resuspended in M9 medium containing 2 g of D-glucose and 1 g of $^{15}NH_4Cl$. The resultant cell cultures were placed back in the shaker incubator and grown until the OD_{600} reached 1.0, at which point protein expression was induced by the addition of IPTG (final concentration of 1 mM). Cells were harvested by centrifugation 3.5 h after induction, and uniformly labeled protein was purified as previously described (*37*). Samples used for NMR data collection consisted of an ~2 mM cytochrome b_5 solution in phosphate buffer [μ (ionic strength) = 0.10, 95% H_2O/5% D_2O, pH 7.0] with 0.05% (w/v) sodium azide.

NMR Spectroscopy. NMR experiments were performed at 30 °C on a Varian Unity INOVA spectrometer operating at a ^1H frequency of 599.73 MHz, equipped with a triple-resonance *z*-axis gradient probe. Data were processed using NMRpipe (*38*) and AutoProc (*39*) and analyzed with the aid of Sparky (T. D. Goddard and D. G. Kneller, *SPARKY 3*, University of California, San Francisco, CA).

Backbone Resonance Assignments of Rat OM Cytochrome b_5. At 30 °C, rOM b_5 exists as a 1:1 mixture of heme orientational isomers that differ by a 180° rotation of the heme about the $\alpha-\gamma$ meso axis. The presence of these two isomers not only causes a virtual doubling of resonances originating from hemin (*37*, *40*) but also results in the doubling of backbone and side chain resonances of several residues in the proximity of the hemin macrocycle. As a result, there are at least 116 backbone N−H cross-peaks in the $^1H-^{15}N$ HSQC spectrum of rOM b_5 (Figure S1 of the Supporting Information) instead of the 88 resonances expected if the five prolines are excluded. The N−H, ^{15}N, C^{α}, C^{β}, C′, and H^{α} resonances from each of the heme orientational isomers (except for residues 41 and −6 to −3) were assigned with the aid of two-dimensional (2D) $^1H-^{15}N$ HSQC, HNCA, CBCACONH, HNCACB, HNCO, HNHA, three-dimensional (3D) $^1H-^{15}N$ NOESY-HSQC, and three-dimensional $^1H-^{15}N$ HMQC-NOESY-HSQC experiments implemented from the Varian BioPack package. Chemical shifts were referenced directly or indirectly to the proton frequency of the DSS resonance at 0.00 ppm (*41*). Chemical shifts are summarized in Table S1 of the Supporting Information.

Backbone Resonance Assignments of Bovine Microsomal Cytochrome b_5. The solution structure of bMc b_5 has been investigated previously (*42*−*44*) using 2D and 3D homonuclear NMR spectroscopy. In addition, the bMc b_5−horse cytochrome *c* (*45*, *46*) and bMc b_5−myoglobin (*47*) complexes have been investigated by high-resolution multidimensional NMR spectroscopy using ^{15}N relaxation and protein docking simulations. Our analysis of the HSQC spectra obtained from bMc b_5 at pH 7.0 and 30 °C was based mainly on assignments previously reported in the literature mentioned above. A comparison of the ^{15}N and ^1H chemical shifts from Mc b_5 obtained in this work (pH 7 and 30 °C) with those reported previously (*42*, *45*) is shown in Table S2 of the Supporting Information. The data show that ^1H and ^{15}N chemical shifts obtained at pH 7 and 30 °C are in good agreement with those reported previously by Hom et al. at pH 6.5 and 25 °C (*45*), with maximum differences of ca. 0.2 ppm in the ^{15}N dimension and ca. 0.1 ppm in the ^1H dimension, which are expected due to the different experimental conditions used in the two studies. There are, however, a few cross-peaks in our HSQC spectra (Asn17, Ser18, Ser20, Leu36, Gly41, and Leu70) whose chemical shifts differ from those reported by Hom et al. (see Table S2). Therefore, cross-peaks from Asn17, Ser18, Ser20, and Leu70 were assigned by comparison to the assignments reported by Musket et al. (*42*) (Table S2). Chemical shifts for Gly41, not reported previously, were assigned by comparison to OM b_5 (Table S1) on the basis of the unique ^1H chemical shift. Leu36 was not assigned. Resonances corresponding to amides in residues Asn16, Phe35, and Asp66 were not used in our HDX analysis due to overlap.

H−D Exchange Studies. Experiments with rOM b_5 were carried out at 30 °C and pD 6.18, 7.07, and 7.92, and experiments with bovine Mc b_5 were performed at 30 °C and pD 6.51, 7.11, and 7.62. For each protein, at least one set of experiments was performed in duplicate. Prior to the start of an HDX experiment, protein samples were exchanged into aqueous sodium phosphate buffer at the appropriate pH and with a μ of 0.10. Samples were then freeze-dried in a Savant (Farmingdale, NY) Speed Vac and subsequently dissolved in 475 μL of D_2O to yield ~2 mM solutions. The dead time between addition of D_2O to lyophilized protein and the beginning of data acquisition ranged between 10 and 15 min. HDX was monitored by following the time-dependent decrease in amide cross-peak intensity with the aid of 2D $^1H-^{15}N$ gHSQC (*48*) spectra. The total acquisition time for each HSQC spectrum (32 increments, eight scans per increment over a 9 kHz spectral width in the ^1H dimension and 2.2 kHz in the ^{15}N dimension, 0.12 s acquisition time, 0.8 s relaxation delay, and 1084 real data points) was approximately 8 min. The HDX experiments were monitored for a total of 72 h by acquiring spectra every 10 min for the first 3 h; subsequent delays between spectra were gradually incremented to a maximum of 12 h. Spectra were transformed with 2168 and 64 data points in the F_2 and F_1 dimensions, respectively. The pD of the D_2O solutions was measured immediately after data acquisition (72 h) and corrected for the deuterium isotope effect according to the relationship $pD_{corrected} = pD_{read} + 0.4$ (*49*), and the corrected value was used in the calculations of k_{ch} (see below). Before the start of a subsequent measurement, the sample was extensively exchanged into aqueous phosphate buffer at the appropriate pH ($\mu = 0.1$). Rate constants for H−D exchange were determined by fitting the time-dependent decay of HSQC cross-peak intensity monitored at each pH to eq 1 (*50*) (see Figure S2) with the aid of SigmaPlot, version 2001.

$$I_t = I_\infty + A \exp(-k_{ex}t) \quad (1)$$

where I_t represents the cross-peak intensity at time t, I_∞ is the cross-peak intensity at infinite time, A represents the

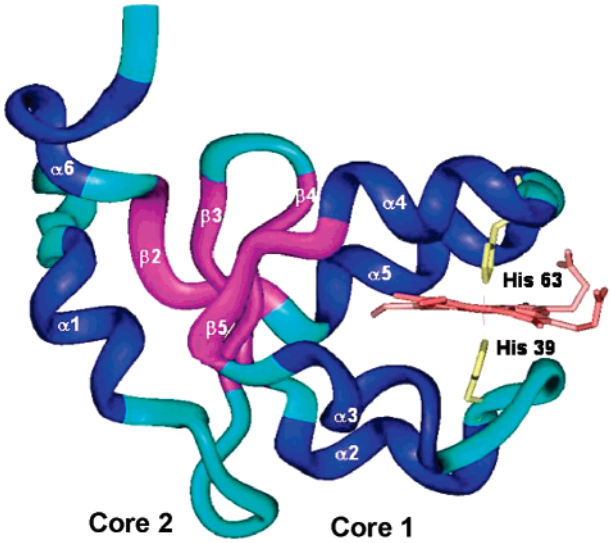

FIGURE 2: Three-dimensional fold of rOM b_5 (PDB entry 1B5M) indicating elements of secondary structure in each of the two hydrophobic cores.

amplitude of the exchange curve, and k_{ex} is the rate constant for N−H exchange characteristic of each residue in the protein. Values for intrinsic rates of exchange (k_{ch}), as well as protection factors and the Gibbs free energy of exchange (ΔG_{HX}) per residue, were calculated utilizing the individual values of k_{ex} and the formulas and spreadsheets available from S. Walter Englander's web page (http://hx2.med.upenn.edu/download.html).

RESULTS AND DISCUSSION

Identification of Elements of Secondary Structure in rOM b_5. The 3D folds of Mc and OM b_5 comprise two crystallographic cores, highlighted in Figure 2 for rOM b_5 (*32*, *33*, *51*). The heme prosthetic group is contained in core 1 which encompasses sequential secondary structure elements α2, turn, α3, β5, α4, turn, and α5, as well as the outer face of β3 and β4. The heme iron is coordinated axially by the N_ϵ atoms of two histidine residues located in the turns between α2 and α3 (His39) and α4 and α5 (His63). Core 2 is composed of two sets of sequential secondary structure elements (β1, α1, β4, and β3 at the N-terminus and β2 and α6 at the C-terminus) and appears to serve a predominantly structural role. These shared elements of secondary structure in Mc and OM b_5s were originally described in the bMc b_5 X-ray crystal structure (*51*), but have also been observed in solution NMR spectroscopic studies of bMc b_5 (*42*−*44*). While several NMR spectroscopic studies aimed at probing the heme active site of rOM b_5 have been reported (*33*, *34*, *40*), this paper reports the first NMR study in which an OM b_5 polypeptide has been probed globally. Work that is in progress toward elucidating the solution structure of rOM b_5 has already shown that the structure in solution compares favorably with that seen in the X-ray crystal structure (*33*). For example, the various elements of secondary structure in solution have been identified from analysis of chemical shift index (CSI) data (*52*, *53*) and from experimental homonuclear $^1H^N-^1H^\alpha$ J values calculated from an HNHA experiment (*54*). Results from CSI analysis of $^{13}C^\alpha$, $^{13}C'$, and $^1H^\alpha$ chemical shifts are summarized in panels A−C of Figure S3 of the Supporting Information, respectively. The data suggest the following: β1 (residues 5−7), α1 (residues 9−14), β4 (residues 22−25), β3 (residues 28−31), α2 (residues 33−38), α3 (residues 44−49), β5 (residues 51−54), α4 (residues 56−61), α5 (residues 65−73), β2 (residues 75−78), and an irregular α6 (residues 82−85). Similar conclusions can be obtained from analysis of $^1H^N-^1H^\alpha$ J values (Figure S4). "Anomalous" $^1H^\alpha$ chemical shift values are observed for residues Gly41 and His63, as well as $^{13}C^\alpha$ chemical shift values for residues His39 and His63, which is a consequence of their proximity (5−6 Å) to the heme iron.

Interpretive Model for the HDX NMR Studies. Amide hydrogen atoms are thought to exchange with deuterium only when a backbone NH makes contact with solvent; thus, eq 2 shows an equilibrium (K_{op}) between closed (exchange incompetent) and open (exchange competent) conformations (*55*, *56*)

$$NH_{(closed)} \underset{k_{cl}}{\overset{k_{op}}{\rightleftharpoons}} NH_{(open)} \xrightarrow[D_2O]{k_{ch}} ND \qquad (2)$$

where k_{op} and k_{cl} represent the rate constants for opening and closing of a structure, respectively, and k_{ch} is the intrinsic rate constant for exchange of a particular NH in the open state. It is generally accepted that values of k_{ch} at a given temperature and pH can be estimated accurately with the approach described by Bai et al. (*57*) utilizing rate constants and equations obtained from unstructured peptides. The experimentally observable rate constant for N−H exchange, k_{ex}, is given by eq 3. When experimental conditions favor the native state of a protein ($k_{cl} \gg k_{ch}$), eq 3 simplifies to eq 4 (EX2 limit), where $K_{op} = k_{op}/k_{cl}$ is the equilibrium constant for the opening reaction (*58*−*61*).

$$k_{ex} = \frac{k_{op}k_{ch}}{k_{cl} + k_{ch}} \qquad (3)$$

$$k_{ex} = K_{op}k_{ch} \qquad (4)$$

Thus, by comparing the experimentally observable rate constant (k_{ex}) to the expected intrinsic rate constant (k_{ch}) for the corresponding NH in its fully exposed condition, we are able to calculate the free energy (ΔG_{HX}) for the dominant opening reaction exposing the site in question (eq 5).

$$\Delta G_{HX} = -RT \ln K_{op} = -RT \ln\left(\frac{k_{ex}}{k_{ch}}\right) \qquad (5)$$

EX2 behavior is characterized by a 10-fold increase in k_{ex} for every unit increase in pH because the intrinsic rate of exchange is catalyzed by the OH^- ion (*55*, *56*). On the other hand, when $k_{cl} \ll k_{ch}$, the EX1 limit, eq 3 simplifies to eq 6, which shows that k_{ex} would depend on only k_{op} and would therefore be pH-independent.

$$k_{ex} = k_{op} \qquad (6)$$

Contrasting Behavior of rOM and bMc b_5. Per residue plots of ΔG_{HX} created from analysis of HDX data obtained with rOM b_5 at 30 °C and pD 6.18, 7.07, and 7.92, as well as with bMc b_5 at 30 °C and pD 6.51, 7.11, and 7.62, are shown in Figure 3. At pD ~7, the number of residues exchanging with rates that are too fast to observe experi-

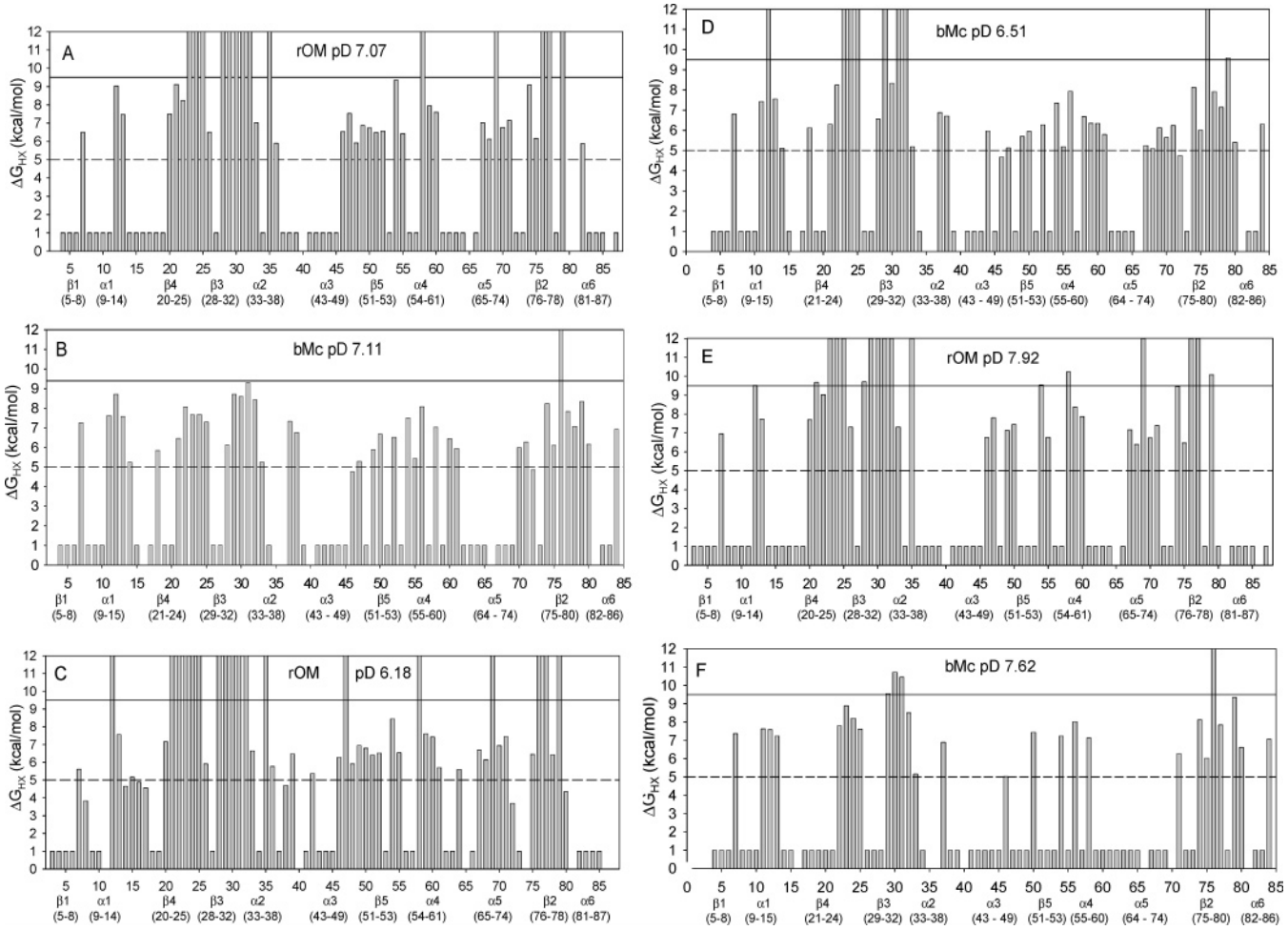

FIGURE 3: Per residue plots of the Gibbs free energy (ΔG_{HX}) obtained for rOM b_5 at 30 °C and (A) pD 7.07, (C) pD 6.18, and (E) pD 7.92. ΔG_{HX} values obtained for bMc b_5 at the same temperature and (B) pD 7.11, (D) pD 6.51, and (F) pD 7.62 are shown for comparison. Vertical bars below the horizontal dashed (5 kcal/mol) line indicate residues exchanging at rates that are too fast to measure, and vertical bars above the horizontal line (9.5 kcal/mol) indicate residues exchanging at rates that are too slow to determine accurately. Those above the 12 kcal/mol line did not undergo observable exchange.

mentally or to measure accurately is approximately 40% in both proteins (Figure 3A,B). The former are represented by the shortest vertical bars in the figures and the latter by all other bars below the horizontal dashed line corresponding to the lower limit value (~5.0 kcal/mol) of ΔG_{HX} that is accessible from experimentally measurable values of k_{ex} (absence of a bar in the figure indicates either that the residue is a Pro or that its backbone NH signal could not be assigned). In rOM b_5 (Figure 3A), this is the case for most residues located in the N- and C-termini and for residues in the turns harboring axial ligands His39 and His63. In bMc b_5 (Figure 3B), residues in the loops containing His39 and His63 are similarly prone to immeasurably rapid exchange. However, bMc b_5 differs from rOM b_5 in having a greater number of residues in helices α3 and α5 and in strand β5 that fall into this category. On the other hand, residues in α1 and β2 of bMc b_5 show a weaker propensity for rapid exchange than rOM b_5 does. The data in panels A and B of Figure 3 show that rOM and bMc b_5 also differ significantly in the number of residues that do not exhibit observable exchange (tallest bars) or that exchange with rates that are too slow to measure accurately (vertical bars above the horizontal line, $\Delta G_{HX} \sim 9.5$ kcal/mol). Approximately 20% of the residues in rOM b_5 exchange with rates that are too slow to measure, mainly those in strands β3 and β4 and some in β2. In comparison, in bMc b_5, the only residue exchanging with a rate too slow to measure is Ile76. These observations taken together suggest a significantly different dynamic behavior among the two b_5 isoforms, despite their almost identical fold.

The contrasting dynamic behavior of the two proteins is made more pronounced by investigating their exchange properties at weakly acidic and weakly basic conditions. When the pH of the solution is lowered, the number of residues in rOM b_5 exchanging with rates too slow to measure scarcely increases from ~20% at pD 7.07 to ~22% at pD 6.18 (Figure 3C). In contrast, the number of residues in bMc b_5 exchanging with immeasurably slow rates increases from ~1% (one residue) at pD 7.11 to ~11% at pD 6.51; these encompass mainly those NHs located in strands β3 and β4 (Figure 3D). Furthermore, the number of residues exchanging at rates too fast to measure in rOM b_5 decreases from ~40% at pD 7.07 to ~30% at pD 6.18, whereas the number of residues exchanging at rates too fast to measure in bMc b_5 remains unchanged (~40%) when the pD is lowered from 7.11 to 6.51. At pD 7.92 (Figure 3E), the number of residues in rOM b_5 exchanging with rates too slow (~20%) or too fast (~40%) to measure remains unchanged relative to that at pH 7.07. In contrast, the number of residues in bMc b_5 exchanging at rates too fast to measure

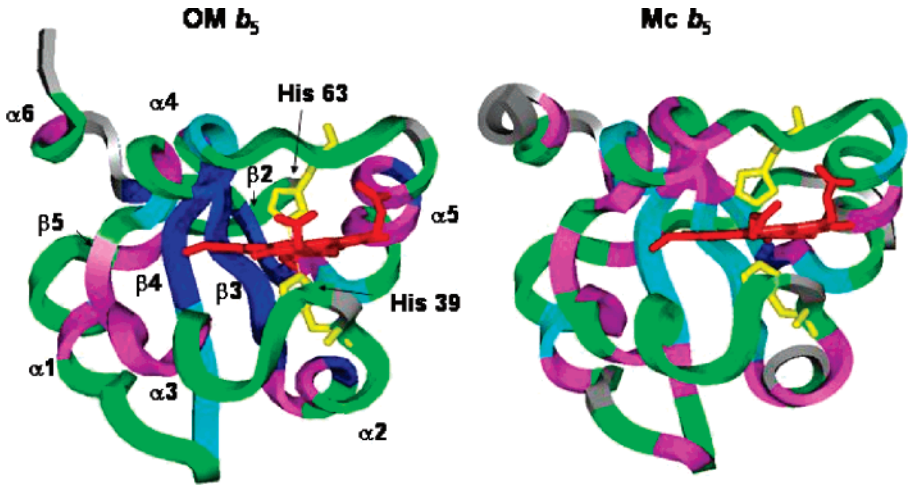

FIGURE 4: Color mapping of ΔG_{HX} values (see panels A and B of Figure 3) on the different elements of secondary structure present in rOM b_5 and Mc b_5. Secondary structure elements harboring NHs exhibiting immeasurably slow rates of exchange ($\Delta G_{HX} > 9.5$ kcal/mol) are colored blue, those for which 9.5 kcal/mol $> \Delta G_{HX} > 7.5$ kcal/mol cyan, NHs for which 7.5 kcal/mol $> \Delta G_{HX} > 5$ kcal/mol pink, and those NHs exhibiting immeasurably fast rates of exchange ($\Delta G_{HX} < 5$ kcal/mol) green. Heme is colored red, and axial ligands His39 and His63 are colored yellow.

increases from ~40% at pD 7.11 to ~65% at pD 7.62, mainly those in α3, β5, and α4 (Figure 3F). These observations clearly indicate that under native conditions rOM b_5 is significantly less prone than bMc b_5 to exploring opening reactions that promote amide hydrogen exchange, despite their almost identical fold. Finally, although in general residues in rOM b_5 exhibit protection factors higher than those exhibited by the corresponding residues in bMc b_5 at all pD values that were studied, there are some noteworthy exceptions: residues 37, 38, and 56 exhibit higher protection factors in bMc b_5 than in rOM b_5 at all pD values that were studied.

The distinctly different dynamic behavior of rOM and bMc b_5 inferred from HDX data at neutral pH is perhaps best illustrated by color coding the results summarized in panels A and B of Figure 3 in the structures of rOM and Mc b_5, respectively. Thus, in Figure 4, elements of secondary structure containing amide hydrogens exhibiting the highest protection factors ($\Delta G_{HX} > 9.5$ kcal/mol) are colored blue, those for which $7.5 < \Delta G_{HX} < 9.5$ cyan, those for which $5 < \Delta G_{HX} < 7.5$ pink, and those exhibiting negligible protection factors ($\Delta G_{HX} < 5$ kcal/mol) green. This analysis reveals that most of the residues located at the bottom of the heme pocket in rOM b_5 ($\beta 2-\beta 4$) are refractory to exchange (Figure 4), whereas amide hydrogens in the equivalent structure of bMc b_5 exchange with measurable rates. As pointed out above, this is one of the most striking differences in the propensity of NH exchange exhibited by the two proteins at all pD values that were studied. In this context, it is interesting to consider that hemin in rOM b_5 is kinetically trapped at 30 °C (*20*), whereas hemin in bMc b_5 is free to undergo reorientation reactions that occur with a rate constant of 0.4 h^{-1} at 24 °C and pH 7.0 (*18*). The rate constant is expected to be larger at 30 °C, which indicates that hemin in bMc b_5 exits and rebinds several times during the course of the HDX experiments described herein. Consequently, it is likely that the resistance to exchange exhibited by NHs at the bottom of the heme pocket in rOM b_5 ($\beta 2-\beta 4$) is imparted by the inertness of hemin toward egress from its binding site. In contrast, for every hemin reorientation event in bMc b_5, if the macrocycle vacates (completely or partially) the heme binding pocket, solvent has access to the interior and facilitates the exchange of residues in $\beta 2-\beta 4$. Subsequent rebinding of hemin expels solvent molecules and therefore protects these groups from exchanging. In the context of this argument, it is interesting to point out that studies by Lecomte and co-workers (*62*−*64*) have shown that core 2 persists as a structured β-barrel ($\beta 1-\beta 4$) when hemin is removed from rat Mc b_5, whereas core 1 is significantly more dynamic and unstructured. Therefore, the observation that NHs in $\beta 2-\beta 4$ in bMc b_5 exhibit relatively high protection factors ($7.5 < \Delta G_{HX} < 9.5$) is consistent with the idea that egress of hemin during the reorientation process leaves behind a structured core 2, where NHs in $\beta 2-\beta 4$ are still protected from very rapid exchange.

Identification of Cooperative Amide Proton Exchange. Analysis of HDX data obtained under EX2 conditions with the aim of investigating cooperative motions can in principle be limited by the fact that a protein must experience several opening transitions before a particular proton is exchanged (eq 2). However, it has been demonstrated that HDX data obtained in the EX2 limit can be efficiently used to identify units (groups of amino acids) exchanging in correlated motions (*65*−*67*). This can be accomplished by analyzing the data in the context of eq 4, which in logarithmic form becomes eq 7.

$$\log k_{ex} = \log k_{ch} + \log\left(\frac{k_{op}}{k_{cl}}\right) \qquad (7)$$

Thus, in logarithmic plots of k_{ex} versus k_{ch}, data points corresponding to amide protons exchanging in cooperative motions with similar populations of the open state should cluster along a straight line with a slope of 1. The intercept of these lines with the log k_{ex} axis when $\log k_{ch} = 0$ provides an estimate of the equilibrium constant (K_{op}) for the opening reaction (*65*, *66*). In contrast, amide hydrogens exchanging via local, uncorrelated fluctuations are not expected to follow a particular pattern. Measuring k_{ex} at several pH values facilitates the identification of cooperative units because the inherent diversity in k_{ch} (~100 fold) (*57*) exhibited by the different residues in a cooperative unit can be extended by

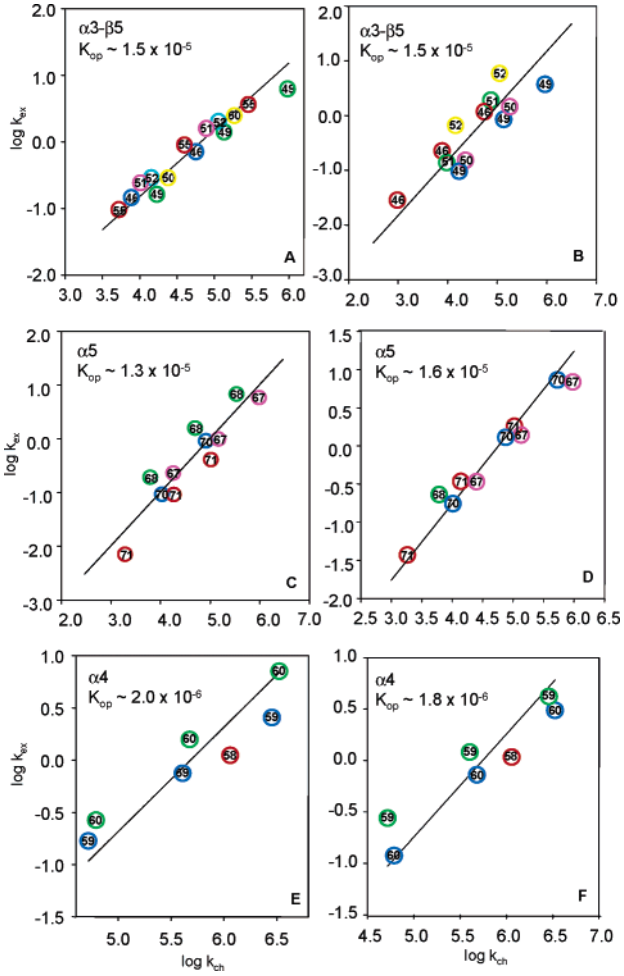

FIGURE 5: Logarithmic plots of k_{ex} (h^{-1}) vs k_{ch} (h^{-1}) constructed with data obtained from rOM b_5 at different pH values. Residues from well-defined elements of secondary structure clustering along a line with a slope of 1 are indicated by numbers inside circles in the different plots. Residues in these clusters share the same intercept of the log k_{ex} axis when log k_{ch} is zero, indicating a common value of K_{op} (see eq 7) and suggesting that these residues exchange in cooperative motions.

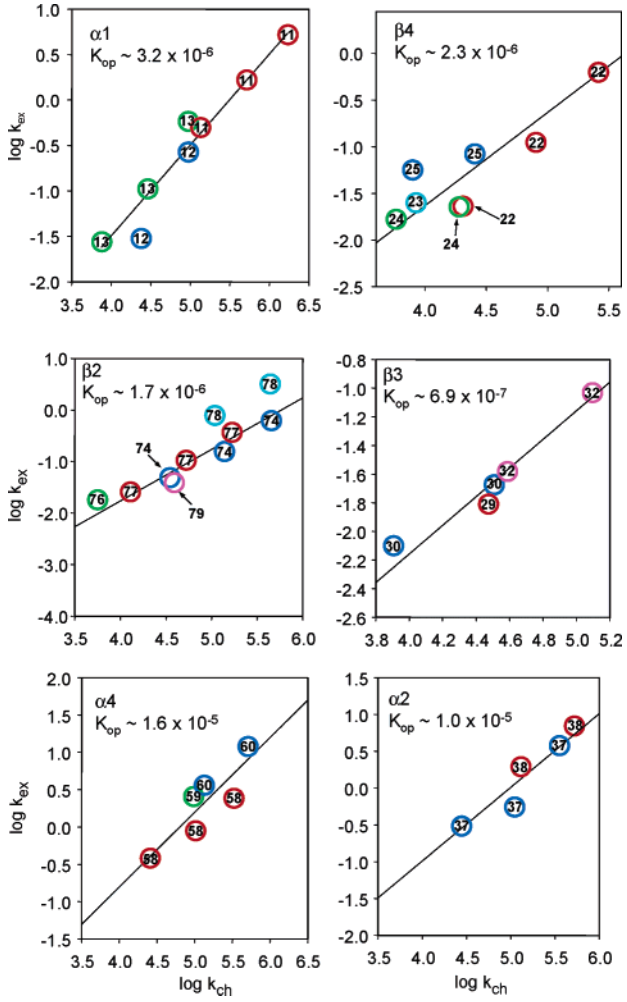

FIGURE 6: Logarithmic plots of k_{ex} (h^{-1}) vs k_{ch} (h^{-1}) constructed with data obtained from bMc b_5 at different pH values. For details, see the legend of Figure 5.

1 order of magnitude for each unit increase in pH (*55*, *57*).

The plots in Figure S5 show that values of log k_{ex} increase approximately 1 order of magnitude for every unit increase in pH for most of the amide hydrogens exchanging at measurable rates. This behavior is indicative of EX2 kinetics and therefore makes it possible to analyze the data in the context of eq 7. This analysis shows that several residues constituting the carboxy-terminal end of α3 and those constituting the adjacent β5 strand in rOM b_5 cluster along a line with a slope of 1 (Figure 5A). Identical observations are made for residues in the second heme orientational isomer in rOM b_5 (Figure 5B), which is populated to an identical extent. The intercept of the lines in panels A and B of Figure 5 (where log $k_{ch} = 0$) suggests that the equilibrium constant for transient unfolding of α3 and β5 in rOM b_5 ($K_{op} = k_{op}/k_{cl} \sim 1.5 \times 10^{-5}$) is insensitive to the orientation of hemin in its binding pocket. Similarly, several residues constituting α5 in each of the two orientational isomers of rOM b_5 cluster along a line with a slope of 1 (Figure 5C,D), and the intercepts suggest a value for K_{op} of $\sim 1.4 \times 10^{-5}$ for transient unfolding of α5, very similar to that exhibited by α3 and β5. These data strongly indicate that the two diastereomeric forms of rOM b_5 exhibit very similar activation barriers for hemin dissociation. This is consistent with our observation that the hemin orientational isomer ratio in rOM b_5 is only 1.2:1 at equilibrium, which can only be achieved by heating a solution of the protein to temperatures above 50 °C (*14*, *20*, *31*). A similar analysis of residues in α4 exchanging at measurable rates in both heme orientational isomers of rOM b_5 (Figure 5E,F) suggests that the C-terminal portion of this helix has a relatively lower propensity to explore the unfolded state ($K_{op} \sim 1.9 \times 10^{-6}$).

Data obtained for bMc b_5 at pH ~7 demonstrate interesting differences relative to rOM b_5. Before proceeding, however, it is important to point out that the two hemin orientational isomers in bMc b_5 exist as a 9:1 equilibrium mixture (*15*, *18*). Consequently, the analysis of resonances and HDX data is concerned only with the most abundant isomer. Most of the residues in α3 and β5 of bMc b_5, and all of the residues in α5, exchange with rates that are too fast to measure (see Figure 3B). Measurable rates of exchange were observed, however, for several residues in β2−β4 of bMc b_5, as well as some residues in α1, α2, and α4. Analysis of these bMc b_5 HDX data in the context of eq 7 shows that exchange rate constants for those residues in helices α1, α2, and α4 and sheet strands β2−β4 cluster along distinct lines with a slope of 1 (Figure 6). The estimated values of K_{op} corresponding to the unfolding of β2, β4, and especially β3 are consistent with strong protection of the corresponding amide

hydrogens, as discussed above. The data also show that residues 37 and 38 in α2, preceding axial ligand His39, exhibit high protection factors, a property not shared by equivalent portions of rOM b_5. The data further indicate that the last residues in α4 (*58*−*60*) in Mc b_5 appear to exchange via a process involving correlated motions, an observation akin to that made with the corresponding residues in rOM b_5 (see panels E and F of Figure 5). It is noteworthy, however, that K_{op} for this segment of α4 in rOM b_5 ($\sim 1.9 \times 10^{-6}$) is approximately 1 order of magnitude smaller than K_{op} in bMc b_5 ($\sim 1.6 \times 10^{-5}$). This difference clearly indicates that this section of α4 in bMc b_5 experiences motions that explore the unfolded state with higher probability than the equivalent section of α4 in rOM b_5. We will come back to this observation later in this report.

Interactions Leading to the High Barrier for Hemin Release in OM b_5. At first glance, and as discussed above, the HDX data show that amide hydrogens in the last turn of α3, extending into β5 in rOM b_5, exhibit relatively high protection factors and appear to exchange in correlated opening reactions (Figures 4 and 5). In comparison, amide hydrogens in similar sections of bMc b_5 are significantly less protected, which suggests a stronger tendency of equivalent portions of α3 and β5 in bMc b_5 to explore unfolding reactions. This is extremely interesting in light of previously reported MD simulations showing that bMc b_5 is more susceptible than rOM b_5 to a large-scale conformational change involving residues in that region. The conformational change was originally reported by Storch and Daggett (*29*), who showed that it causes a substantial increase in the distance between Ser18 (at the center of a surface-exposed loop in core 1) and Ala50 (bridging the end of α3 and the beginning of β5 in core 2). The reversible conformational change created a cleft that exposed several internal residues to the aqueous environment. An analogous study in Kuczera's laboratory (*9*, *30*) showed that the changes in core 2 leading to the cleft involved, in addition to Ala50, the last residue in α3 (Gln49) and the first two residues in β5 (Gly51 and Gly52). In contrast, MD studies of rOM b_5 showed that an analogous cleft did not form. It is interesting that, despite the very different time scales probed by MD simulations and HDX experiments, the exchange data presented herein also reveal a significantly weaker tendency in α3 and β5 of OM b_5 to explore unfolded (exchange competent) states than in bMc b_5.

Differences in the identity of the residue occupying position 47 in α3 of rOM b_5 (Leu) and bMc b_5 (Arg) may contribute substantially to the different susceptibility of the two proteins to undergo a cleft-opening event. Leu47 lies at the surface of rOM b_5, and is a key contributor to one of the two conserved OM b_5 hydrophobic patches mentioned in the introductory section. The Leu47 side chain forms a hydrophobic packing interaction with the side chain of Ala18, which is located in a core 2 surface loop between α1 and β4. The Leu47 side chain also makes van der Waals contact with the buried side chain of Leu36 in α2, which in turn interacts with the buried side chain of Ile32 in β3. Interactions among the corresponding residues in bMc b_5 (Arg47, Ser18, Leu36, and Leu32) offer much less extensive hydrophobic packing. While the side chains of Arg47 and Ser18 form a polar interaction in the X-ray crystal structure of bMc b_5, that conformation is only rarely occupied in MD simulations of the protein. Furthermore, in the A18S/I32L/L47R triple mutant of rOM b_5, the Arg47 side chain favors formation of an intrahelical salt bridge with the side chain of Glu43.

The lower conformational flexibility of the last turn of α3 extending into β5 in rOM b_5 than in bMc b_5 might also be due in part to the only difference in the sequence of amino acids defining β5 in the two proteins. In rOM b_5, residue 52 is an Ala, whereas in bMc b_5, it is a Gly. Residue 51 in both proteins is also a Gly. Because Gly is able to explore a greater range of backbone torsional angles than Ala, one might anticipate that β5 in bMc b_5 will have a markedly stronger tendency to sample multiple conformations than will β5 in rOM b_5. The side chain of Ala52 in rOM b_5 also packs against the methylene group in the side chain of Gln49 in α3 (Figure S6A), a potentially stabilizing interaction that is not possible in bMc b_5 despite the fact that it also contains Gln at position 49. Additional stabilization for β5 of rOM b_5 in comparison to bMc b_5 may arise from a difference in the identity of the amino acid at position 57 in α4 (Ser in rOM b_5 and Asn in bMc b_5). The side chain of Gln49 in α3 of rOM b_5 reaches across to the hydroxyl group of Ser57 in α4 and forms a hydrogen bond. Similar interactions are not observed in the structure of bMc b_5 because the side chains of Gln49 and Asn57 are too close to form a hydrogen bond (Figure S6B).

The local differences in packing interactions among residues 49, 52, and 57 in α3, β5, and α4 of bMc and rOM b_5, together with differences in hydrophobic packing interactions emanating from nearby residue 47 in α3, might be expected to be manifested in different dynamic behaviors of the two proteins that extend throughout core 1. Our HDX data suggest that this is indeed the case. For example, a series of strong H-bonds involving residues in α4 of rOM b_5 is observed which can be described as follows. The NHs from Phe58 and Glu59 form strong hydrogen bonds with the carbonyl oxygens of Ala54 and Thr55, respectively (Figure 7). In turn, the NHs of Ala54 and Thr55, which also exhibit high protection factors at all pH values that were studied, form hydrogen bonds to the carbonyl oxygen of Val24 and the side chain carbonyl oxygen of Asp53, respectively. A conformationally restricted β5 in rOM b_5 may therefore potentially limit the mobility of the Asp53 backbone, while hydrophobic interactions between the side chains of Asp53 and Val24 may further restrict the conformation of the Asp53 side chain. Together, these interactions may stabilize the hydrogen bond to the NH of Thr55, representing a possible source of its high protection against exchange at all pH values that were studied. In contrast, HDX data indicate that α3 and β5 in bMc b_5 are more conformationally dynamic, as manifested by comparatively lower protection factors, i.e., weaker hydrogen bonding interactions in α4. Hence, although the structure of bMc b_5 shows similar hydrogen bonds in helix α4 relative to those just described in rOM b_5, the propensity of these NHs to exchange in Mc b_5 is significantly more pronounced. For instance, the NH of Glu59 exchanges very rapidly at neutral pH, the NH of Thr55 exchanges immeasurably fast at pH 7.18 and 7.92 and exhibits a very low protection factor at pH 6.5, and the NH of Ala54 is relatively protected toward exchange.

On this basis, it is reasonable to conclude that an important outcome of reduced conformational disorder in α3 and β5

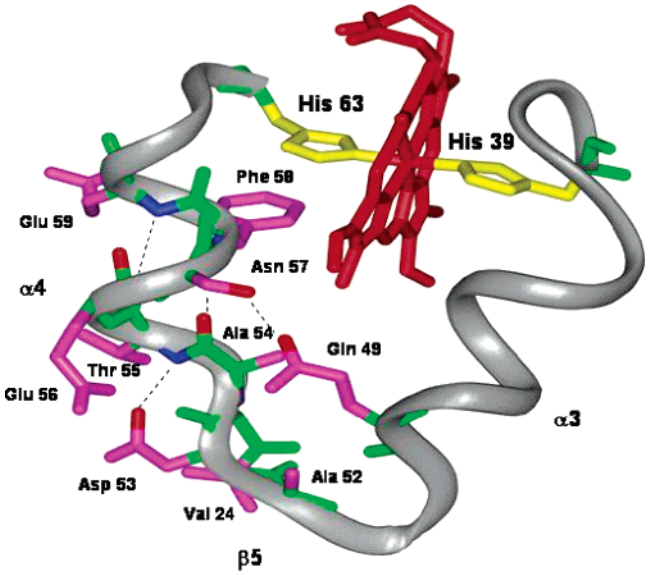

FIGURE 7: View of a portion of the rOM b_5 structure illustrating how stability in α3 and β5 is propagated via hydrogen bonds involving amide hydrogens exhibiting high protection factors. This view also illustrates the face-to-face π-stacking interactions between the side chains of Phe58 and axial ligand His63. Heme is colored red, and axial ligands are colored yellow, side chains pink, carbonyl oxygens red, amide nitrogens blue, and backbone atoms green.

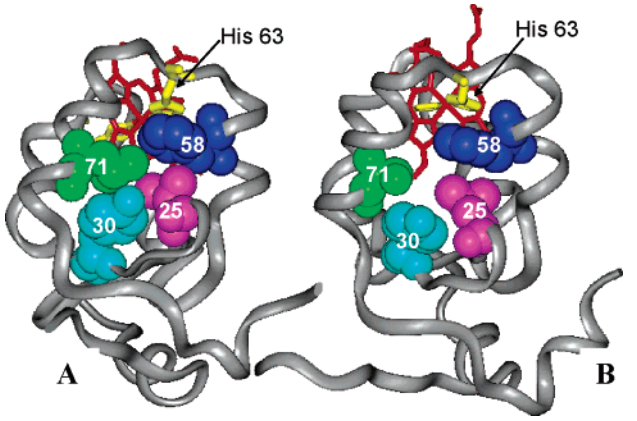

FIGURE 8: (A) View of rOM b_5 highlighting interactions among residues Ile25, Tyr30, Phe58, and Leu71. (B) Similar view of bMc b_5 highlighting interactions among Leu25, Phe30, Phe58, and Ser71 in bMc b_5. Heme is colored red, and axial ligands His39 and His63 are colored yellow.

of rOM b_5, propagated along α4 via key interactions, results in the restricted conformational flexibility of Phe58. The latter is evident from its very high protection factor at all pH values that were studied. The significance of this observation is illuminated by inspection of the structure of rOM b_5, which shows that the side chain of Phe58 engages in edge-to-face aromatic interactions with the heme and in π-stacking interactions with the imidazolyl side chain of heme ligand His63 (Figure 7). In addition, the backbone carbonyl oxygen of Phe58 forms a hydrogen bond with the side chain NH of His63. These interactions may be conceived to act in synergism to minimize the conformational mobility of His63. Therefore, the lower mobility of α3 and β5 in rOM b_5 than in bMc b_5 may ultimately be manifested in a stronger His63−Fe coordination bond in the mitochondrial isoform. This, in turn, could lead to a lower propensity for hemin to egress from rOM b_5. The comparatively greater conformational freedom of α3 and β5 in bMc b_5 may be ultimately manifested in greater conformational freedom of Phe58, which may lead to relatively lower stability of the His63−Fe coordination bond. It should also be mentioned that the role of a relatively stable α4 in maintaining hemoprotein stability and in lowering the propensity for hemin release is in agreement with the approximately 1 order of magnitude smaller K_{op} for α4 in rOM b_5 relative to bMc b_5 (Figures 5 and 6) and with a recent report indicating that destabilization of α4 results in a protein with a significantly lower affinity for hemin (*68*).

Further analysis of HDX data provides additional insights into the characteristically low propensity of rOM b_5 to release hemin. These findings stem from the observation that several NHs in α5 of rOM b_5 exhibit relatively high protection factors at all pH values that were studied. Noteworthy among these residues is the NH of Glu69 (center of α5) which exhibits immeasurably slow rates of exchange at all pH values. Inspection of the structure reveals that the Glu69 NH forms a hydrogen bond with the carbonyl oxygen of Pro65 and strongly suggests that the very strong protection of the Glu69 NH toward exchange is imparted by the low conformational mobility of Pro65. Furthermore, the side chain of neighboring residue Arg68 in α5 forms an H-bond with that of Glu59 in α4, whose backbone NH also has an immeasurably slow rate of exchange, suggesting an additional possible contributor to the lower mobility near His63 of rOM b_5 than of bMc b_5. Thr occupies position 65 in bMc b_5, which cannot provide such an "anchoring" effect.

An additional factor contributing to the higher stability of α5 in rOM b_5 is the presence of a second hydrophobic network present in OM b_5s but absent in Mc b_5s (*10*, *14*). One way of describing this hydrophobic network in rOM b_5 (Figure 8A) starts with Leu71, located in the final turn of α5, which makes hydrophobic contact with Phe58, located in the opposing helix α4, and with Ile25, harbored by strand β4. Leu71 and Ile25 also make hydrophobic contact with Tyr30, located at the bottom of the heme pocket in strand β3. This hydrophobic network is extended by van der Waals contacts between the heme and side chains of residues 25, 58, and 71. A similar view of bMc b_5 (Figure 8B) indicates that the tightly knit hydrophobic network of the rOM protein is absent in the Mc isoform. The absence of an equivalent hydrophobic network in Mc b_5s originates from the presence of Leu at position 25 and Ser at position 71, which results in a cavity that permits water to access the heme (*14*). Replacement of Ile25 and Leu71 in rOM b_5 with their equivalent residues in Mc b_5 (Leu and Ser, respectively) opened a similar cavity in the structure of the rOM mutant. The structural changes were accompanied by a concomitant decrease in stability and a modest increase in the tendency to release hemin relative to the wild-type protein (*14*). It is therefore likely that the markedly higher protection factors in α5 of rOM b_5 are in part a consequence of propagation of the lower conformational flexibility in the hydrophobic network shown in Figure 8A via Leu71. This kind of stabilization is clearly not possible in bMc b_5.

When all the information given above is put together, the picture that emerges indicates that the two hydrophobic networks unique to OM b_5 contribute to lowering the conformational flexibility in the last turn of α3, the entirety of β5, and most of α5. The influence of α3 and β5 is

propagated via key interactions along α4, whereas α5 is stabilized by the presence of Pro65 on one side of the helix and the participation of Leu71 in key hydrophobic interactions on the opposite side. An important consequence of these interactions in rOM b_5 is the stabilization of the two helical segments leading into the loop containing His63 (α4 and α5), which lowers the propensity of these two helical segments to melt (see Figure 4), therefore contributing to a stronger Fe−His63 coordination bond. An additional but related manner in which the Fe−His63 bond is stabilized in rOM b_5 is by strong restriction of the conformational mobility of Phe58 in α4. Restricted backbone and side chain conformational mobility in Phe58, in turn, restricts the conformational mobility of the His63 imidazolyl side chain and likely contributes to a stronger coordination bond.

It is also interesting to observe that in contrast to the relatively restricted conformational dynamics in elements of secondary structure leading to the loop harboring His63, elements of secondary structure leading to the loop containing the other axial ligand, His39, are more prone to undergoing unfolding reactions. The latter is manifested in immeasurably fast rates of exchange for the latter part of α2, which leads toward the loop containing His39 and the equally fast exchange of NHs in the first half of α3, which leads away from this loop (Figure 4). This suggests that compared to His63, His39 is more susceptible to undergoing conformational fluctuations which would ultimately reduce the strength of the Fe−His39 coordination bond. Hence, it is tempting to hypothesize that release of hemin from cytochrome b_5 would start by dissociation of the Fe−His39 coordination bond. For hemin to be released, dissociation of the Fe−His63 bond would have to occur before rebinding of His39 occurs. The relatively low conformational flexibility of the helices leading to the loop containing His63 suggests that in rOM b_5 rebinding of His39 is a more probable event than dissociation of His63, thus explaining the kinetic trapping of hemin in this molecule. In comparison, the relatively large conformational flexibility in the neighborhood of His63 in Mc b_5 suggests that dissociation of the Fe−His63 bond would occasionally occur before rebinding of His39. This situation would allow hemin egress and therefore hemin reorientation. Although this hypothesis awaits further experimentation, it finds support in conclusions obtained from kinetic studies carried out with axial ligand mutants of rat Mc b_5 which indicated that the first step in heme binding proceeds via the initial coordination of His63 (*69*) and from the fact that in Mc b_5 replacement of His39 results in a protein with higher affinity for hemin than replacement of His63 (*69*, 70).

Concluding Remarks. Previous investigations in our laboratories aimed at understanding the distinct biochemical and biophysical properties of rOM and bMc b_5s were carried out on the basis of amino acid sequence comparisons in the context of their three-dimensional structures. This approach allowed identification of two hydrophobic clusters in OM b_5s that are less extensive in the Mc isoforms. Our studies in which key residues contributing to those clusters in rOM b_5 were replaced with the corresponding residues characteristic of Mc b_5s demonstrated that they play a role in the greater stability and higher hemin release barriers of the OM proteins (*9*, *14*). They did not, however, provide direct insight into the way in which interactions within those clusters render OM b_5s with less structural plasticity than Mc b_5s. Our interest in delineating the relationship between structure and dynamics is related to our long-term goal of understanding how they govern functional properties. For example, OM b_5s may have evolved to interact with a relatively limited set of physiological partners in comparison to Mc b_5s, and might therefore have less need for adaptability via surface conformational mobility. In this context, the correspondingly low hemin release barriers of Mc b_5s may be an interesting but functionally irrelevant consequence of developing surface conformational plasticity that allows interactions with diverse physiological partners. Another possibility that we have entertained is that the more negative reduction potentials exhibited by OM b_5s in comparison to their Mc counterparts, which provide a stronger driving force for electron delivery, are a direct consequence of their greater stability and lower dynamic mobility. In this context, it is noteworthy that studies with synthetic bis-histidine-coordinated heme peptides have shown that structural changes which diminish peptide conformational mobility result in greater stabilization of His−Fe(III) coordination than of His−Fe(II) coordination and therefore a negative shift in reduction potential (*71*, *72*). Studies aimed at comparing stability and dynamic properties of bMc and rOM b_5 in the ferrous oxidation state are presently underway in our laboratories.

ACKNOWLEDGMENT

We are thankful to Frank Delaglio (National Institutes of Health, Bethesda, MD) for advice with NMRpipe, Gaetano T. Montelione, James M. Aramini, and Marvin Byro (Rutgers University, New Brunswick, NJ) for assistance with AutoProc, and Thomas Goddard (University of California, San Francisco, CA) for assistance with Sparky.

SUPPORTING INFORMATION AVAILABLE

$^1H-^{15}N$ HSQC spectrum of ferric rat OM b_5 (Figure S1), time-dependent decrease of cross-peak intensity (Figure S2), summary of chemical shift index data (Figure S3), per residue plots of $^1H^N-^1H^\alpha$ *J* values (Figure S4), plots of log k_{ex} versus pD (Figure S5), view of interactions among residues 49, 52, and 57 in rOM b_5 and bMc b_5 (Figure S6), ^1H, C', C^α, C^β, and H^α chemical shifts for rat ON b_5 (Table S1), and comparison of ^1H and ^{15}N chemical shifts for bovine MC b_5 (Table S2). This material is available free of charge via the Internet at http://pubs.acs.org.

REFERENCES

1. Yoo, M., and Steggles, A. W. (1988) The Complete Nucleotide Sequence of Human Liver Cytochrome b_5 mRNA, *Biochem. Biophys. Res. Commun. 156*, 576−580.
2. Cristiano, R. J., and Steggles, A. W. (1989) The Complete Nucleotide Sequence of Bovine Liver Cytochrome b_5 mRNA, *Nucleic Acids Res. 17*, 799.
3. VanDerMark, P., and Steggles, A. W. (1997) The Isolation and Characterization of the Soluble and Membrane-Bound Porcine Cytochrome b_5 cDNAs, *Biochem. Biophys. Res. Commun. 240*, 80−83.
4. Strittmatter, P. (1967) Cytochrome b_5, *Methods Enzymol. 10*, 553.
5. Porter, T. D. (2002) The roles of Cytochrome b_5 in Cytochrome P450 Reactions, *J. Biochem. Mol. Toxicol. 16*, 311−316.
6. Vergeres, G., and Waskell, L. (1995) Cytochrome b_5, its functions, structure and membrane topology, *Biochimie 77*, 604−620.
7. Ito, A. (1980) Cytochrome b_5-Like Hemoprotein of Outer Mitochondrial Membrane; OM Cytochrome b, *J. Biochem. 87*, 63−71.

8. Kuroda, R., Ikenoue, T., Honsho, M., Tsujimoto, S., Mitoma, J., and Ito, A. (1998) Charged Amino Acids at the Carboxy-Terminal Portions Determine the Intracellular Locations of Two Isoforms of Cytochrome b_5, *J. Biol. Chem. 273*, 31097−31102.
9. Altuve, A., Silchenko, S., Lee, K. H., Kuczera, K., Terzyan, S., Zhang, X., Benson, D. R., and Rivera, M. (2001) Probing the Differences Between Rat Liver Outer Mitochondrial Membrane Cytochrome b_5 and Microsomal Cytochromes b_5, *Biochemistry 40*, 9469−9483.
10. Altuve, A., Wang, L., Benson, D. R., and Rivera, M. (2004) Mammalian Mitochondrial and Microsomal Cytochromes b_5 Exhibit Divergent Structural and Biophysical Characteristics, *Biochem. Biophys. Res. Commun. 305*, 840−845.
11. Rivera, M., Wells, M. A., and Walker, F. A. (1994) Cation-Promoted Cyclic Voltammetry of Recombinant Rat Outer Mitochondrial Membrane Cytochrome b_5 at a Gold Electrode Modified with β-Mercaptopropionic Acid, *Biochemistry 33*, 2161−2170.
12. Wirtz, M., Oganesyan, V., Zhang, X., Studer, J., and Rivera, M. (2000) Modulation of Redox Potential in Electron Transfer Proteins: Effects of Complex Formation on the Active Site Microenvironment of Cytochrome b_5, *Faraday Discuss. 116*, 221−234.
13. Rivera, M., Seetharaman, R., Ghirdhar, D., Wirtz, M., Zhang, X., Wang, X., and White, S. (1998) The Reduction Potential of Cytochrome b_5 is Modulated by Its Exposed Heme Edge, *Biochemistry 37*, 1485−1494.
14. Cowley, A. B., Altuve, A., Kuchment, O., Terzyan, S., Zhang, X., Rivera, M., and Benson, D. R. (2002) Toward Engineering the Stability and Hemin-Binding Properties of Microsomal Cytochromes b_5 in Rat Mitochondrial Membrane Cytochrome b_5: Examining the Influence of Residues 25 and 71, *Biochemistry 41*, 11566−11581.
15. La Mar, G. N., Burns, P. D., Jackson, J. T., Smith, K. M., Langry, K. C., and Strittmatter, P. (1981) Proton Magnetic Resonance Determination of the Relative Heme Orientations in Disordered Native and Reconstituted Ferricytochrome b_5, *J. Biol. Chem. 256*, 6075−6079.
16. McLachlan, S. J., La Mar, G. N., and Sletten, E. (1986) Ferricytochrome b_5: Assignments of Heme Propionate Resonances on the Basis of Nuclear Overhauser Effect Measurements and the Nature of Interprotein Contacts with Partner Redox Proteins, *J. Am. Chem. Soc. 108*, 1285−1291.
17. McLachlan, S. J., La Mar, G. N., Burns, P. D., Smith, K. M., and Langry, K. C. (1986) ^{1}H NMR Assignments and the Dynamics of Interconversion of the Isomeric Forms of Cytochrome b_5 in Solution, *Biochim. Biophys. Acta 874*, 274−284.
18. Walker, F. A., Emrick, D., Rivera, J. E., Hanquet, B. J., and Buttlaire, D. H. (1988) Effect of Heme Orientation on the Reduction Potential of Cytochrome b_5, *J. Am. Chem. Soc. 110*, 6234−6240.
19. Mortuza, G. B., and Whitford, D. (1997) Mutagenesis of Residues 27 and 78 Modulates Heme Orientation in Cytochrome b_5, *FEBS Lett. 412*, 610.
20. Silchenko, S., Sippel, M. L., Kuchment, O., Benson, D. R., Mauk, A. G., Altuve, A., and Rivera, M. (2000) Hemin is Kinetically Trapped in Cytochrome b_5 from Rat Outer Mitochondrial Membrane, *Biochem. Biophys. Res. Commun. 273*, 467−472.
21. Ito, A., Hayashi, S., and Yoshida, T. (1981) Participation of a Cytochrome b_5-Like Hemoprotein of Outer Mitochondrial Membrane (OM Cytochrome b) in NADH−Semidehydroascorbic Acid Reducatase Activity, *Biochem. Biophys. Res. Commun. 101*, 591−598.
22. Ogishima, T., Kinoshita, J., Mitani, F., Suematsu, M., and Ito, A. (2003) Identification of Outer Mitochondrial Membrane Cytochrome b_5 as a Modulator of Androgen Synthesis in Leydig Cells, *J. Biol. Chem. 278*, 21204−21211.
23. Soucy, P., and Luu-The, V. (2002) Assessment of the ability of type 2 cytochrome b_5 to modulate 17,20-lyase activity of human P450c17, *J. Steroid Biochem. Mol. Biol. 80*, 71−75.
24. Reid, L. S., and Mauk, A. G. (1982) Kinetic Analysis of Cytochrome b_5 Reduction by Fe(EDTA)$^{2-}$, *J. Am. Chem. Soc. 104*, 841−845.
25. Rodgers, K. K., and Sligar, S. G. (1991) Mapping Electrostatic Interactions in Macromolecular Associations, *J. Mol. Biol. 221*, 1453−1460.
26. Berendsen, J. C., and Hayward, S. (2000) Collective Protein Dynamics in Relation to Function, *Curr. Opin. Struct. Biol. 10*, 165−169.
27. Miller, D. W., and Agard, D. A. (1999) Enzyme Specificity Under Dynamic Control: A Normal Mode Analysis of α-Lytic Protease, *J. Mol. Biol. 286*, 267−278.
28. Pochapsky, S. S., Pochaspsky, T. C., and Wei, J. W. (2003) A Model for Effector Activity in a Highly Specific Biological Electron Transfer Complex: The cytochrome $P450_{cam}$-Putidaredoxin Couple, *Biochemistry 42*, 5649−5656.
29. Storch, E. M., and Daggett, V. (1995) Molecular Dynamics Simulation of Cytochrome b_5: Implications for Protein−Protein Recognition, *Biochemistry 34*, 9682−9693.
30. Lee, K. H., and Kuczera, K. (2003) Molecular Dynamics Simulation Studies of Cytochrome b_5 from mitochondrial and microsomal membrane, *Biopolymers 69*, 260−269.
31. Cowley, A. B., Rivera, M., and Benson, D. R. (2004) Stabilizing roles of residual structure in the empty heme binding pockets and unfolded states of microsomal and mitochondrial apocytochrome b_5, *Protein Sci. 13*, 2316−2329.
32. Durley, R. C. E., and Mathews, F. S. (1996) Refinement and Structural Analysis of Bovine Cytochrome b_5 at 1.5 Å Resolution, *Acta Crystallogr. D52*, 65−76.
33. Rodriguez-Maranon, M. J., Feng, Q., Stark, R. E., White, S. P., Zhang, X., Foundling, S. I., Rodriguez, V., Schilling, C. L., III, Bunce, R. A., and Rivera, M. (1996) ^{13}C NMR Spectroscopic and X-ray Crystallographic Study of the Role Played by Mitochondrial Cytochrome b_5 Heme Propionates in the Electrostatic Binding to Cytochrome *c*, *Biochemistry 35*, 16378−16390.
34. Rivera, M., Caignan, G. A., Astashkin, A. V., Raitsimring, A. M., Shokhireva, T. K., and Walker, F. A. (2002) Models of the Low-Spin Iron(III) Hydroperoxide Intermediate of Heme Oxygenase: Magnetic Resonance Evidence for Thermodynamic Stabilization of the d_{xy} Electronic State at Ambient Temperatures, *J. Am. Chem. Soc. 124*, 6077−6089.
35. Funk, W. D., Lo, T. P., Mauk, M. R., Brayer, G. D., MacGillivray, R. T. A., and Mauk, G. M. (1990) Mutagenic, Electrochemical and Crystallographic Investigation of the Cytochrome b_5 Oxidation−Reduction Equilibrium: Involvement of Asparagine-57, Serin-64 and Heme Propionate-7, *Biochemistry 29*, 5500−5508.
36. Rodriguez, J. C., and Rivera, M. (1998) Conversion of Mitochondrial Cytochrome b_5 into a Species Capable of Performing the Efficient Coupled Oxidation of Heme, *Biochemistry 37*, 13082−13090.
37. Rivera, M., Barillas-Mury, C., Christensen, K. A., Little, J. W., Wells, M. A., and Walker, F. A. (1992) Gene Synthesis, Bacterial Expression, and ^{1}H NMR Spectroscopic Studies of the Rat Outer Mitochondrial Membrane Cytochrome b_5, *Biochemistry 31*, 12233−12240.
38. Delaglio, F., Grzesiek, S., Vuister, G. W., Zhu, W., Pfeifer, J., and Bax, A. (1995) NMRPipe: A Multidimensional Spectral Processing System Based on UNIX pipes, *J. Biomol. NMR 6*, 277−293.
39. Monleón, D., Colson, K., Moseley, H. N. B., Anklin, C., Oswald, R., Szyperski, T., and Montelione, G. T. (2002) Rapid Analysis of Protein Backbone Resonance Assignments Using Cryogenic Probes, a Distributed Linux-Based Computing Architecture, and an Integrated Set of Spectral Analysis Tools, *J. Struct. Funct. Genomics 2*, 93−101.
40. Rivera, M., Qiu, F., Bunce, R. A., and Stark, R. E. (1999) Complete Isomer-Specific ^{1}H and ^{13}C NMR Assignments of the Heme Resonances of Rat Liver Outer Mitochondrial Membrane Cytochrome b_5, *J. Biol. Inorg. Chem. 4*, 87−98.
41. Wishart, D. S., Bigam, C. G., Yao, J., Abildgaard, F., Dyson, H. J., Oldfield, E., Markley, J. L., and Sykes, B. D. (1995) ^{1}H, ^{13}C and ^{15}N Chemical Shift Referencing in Biomolecular NMR, *J. Biomol. NMR 6*, 135−140.
42. Muskett, F. W., Kelly, G. P., and Whitford, D. (1996) The Solution Structure of Bovine Ferricytochrome b_5 Determined Using Heteronuclear NMR Methods, *J. Mol. Biol. 258*, 172−189.
43. Veitch, N. C., Concar, D. W., Williams, R. J. P., and Whitford, D. (1988) Investigation of the Solution Structures and Mobility of Oxidised and Reduced Cytochorme b_5, *FEBS Lett. 238*, 49−55.
44. Kelly, G. P., Muskett, F. W., and Whitford, D. (1997) Analysis of Backbone Dynamics in Cytochrome b_5 Using ^{15}N NMR Relaxation Measurements, *Eur. J. Biochem. 245*, 349−354.
45. Hom, K., Ma, Q.-F., Wolfe, G., Zhang, H., Storch, E. M., Daggett, V., Basus, V. J., and Waskell, L. (2000) NMR Studies of the Association of Cytochrome b_5 with Cytochrome c, *Biochemistry 39*, 14025−14039.

46. Shao, W., Im, S.-C., Zuiderweg, R. P., and Waskell, L. (2003) Mapping the Binding Interface of the Cytochrome b_5−Cytochrome *c* Complex by Nuclear Magnetic Resonance, *Biochemistry 42*, 14774−14784.
47. Worrall, J. A. R., Liu, Y., Crowley, P. B., Nocek, J. M., Hoffman, B. M., and Ubbink, M. (2003) Myoglobin and Cytochrome b_5: A Nuclear Magneic Resonance Study of a Highly Dynamic Protein Complex, *Biochemistry 42*, 7068−7076.
48. Kay, L. E., Keifer, P., and Saarinen, T. (1992) Pure Absorption Gradient Enhanced Heteronuclear Single Quantum Correlation Spectroscopy with Improved Sensitivity, *J. Am. Chem. Soc. 114*, 10663−10665.
49. Glasoe, P. K., and Long, F. A. (1960) Use of Glass Electrodes to Measure Acidities in Deuterium Oxide, *J. Phys. Chem. 64*, 188−190.
50. Swint-Kruse, L., and Robertson, A. D. (1996) Temperature and pH Dependences of Hydrogen Exchange and Global Stability for Ovomucoid Third Domain, *Biochemistry 35*, 171−180.
51. Mathews, F. S., Gerwinsky, E. W., and Argos, P. (1979) in *The Porphyrins, 7, The X-ray Crystallographic Structure of Calf Liver Cytochrome b_5* (Dolphin, D., Ed.) pp 107−147, Academic Press, New York.
52. Wishart, D. S., and Sykes, B. D. (1994) The ^{13}C Chemical-Shift Index: A Simple Method for the Identification of Protein Secondary Structure Using ^{13}C Chemical Shift Data, *J. Biomol. NMR 4*, 171−180.
53. Wang, Y., and Jardetzky, O. (2002) Probability-Based Protein Secondary Structure Identfication Using Combined NMR Chemical Shift Data, *Protein Sci. 11*, 852−861.
54. Vuister, G. W., and Bax, A. (1993) Quantitative J Correlation: A New Approach for Measuring Homonuclear Three-Bond $J_{HN-H\alpha}$ Coupling Constants in ^{15}N-Enriched Proteins, *J. Am. Chem. Soc. 115*, 7772.
55. Hvidt, A., and Nielsen, S. O. (1966) in *Advances in Protein Chemistry, 21, Hydrogen Exchange in Proteins* (Anfinsen, C. B., Lanson, M. L., Edsall, J. T., and Richards, F. M., Eds.) pp 288−380, Academic Press, New York.
56. Bai, Y., Milne, J. S., Mayne, L., and Englander, S. W. (1994) Protein Stability Parameters Measured by Hydrogen Exchange, *Proteins: Struct., Funct., Genet. 20*, 4−14.
57. Bai, Y., Milne, J. S., Mayne, L., and Englander, S. W. (1993) Primary Structure Effects on Peptide Group Hydrogen Exchange, *Proteins: Struct., Funct., Genet. 17*, 75−86.
58. Bai, Y., Sosnick, T., Mayne, L., and Englander, S. W. (1995) Protein Folding Intermediates: Native-State Hydrogen Exchange, *Science 269*, 192−197.
59. Arrington, C. B., Teesch, L. M., and Robertson, A. D. (1999) Defining Protein Ensembles with Native-state NH Exchange: Kinetics of Interconversion and Cooperative Units from Combined NMR and MS Analysis, *J. Mol. Biol. 285*, 1265−1275.
60. Englander, S. W., and Krishna, M. G. (2001) Hydrogen Exchange, *Nat. Struct. Biol. 8*, 1−2.
61. Bahar, I., Wallqvist, A., Covell, D. G., and Jernigan, R. L. (1998) Correlation Between Native-State Hydrogen Exchange and Cooperative Residue Fluctuations from a Simple Model, *Biochemistry 37*, 1067−1075.
62. Moore, C. D., and Lecomte, J. T. J. (1993) Characterization of an Independent Structural Unit in Apocytochrome b_5, *Biochemistry 32*, 199−207.
63. Moore, C. D., and Lecomte, J. T. J. (1990) Structural Properties of Apocytochrome b_5: Presence of a Stable Native Core, *Biochemistry 29*, 1984−1989.
64. Falzone, C. J., Mayer, M. R., Whiteman, E. L., Moore, C. D., and Lecompte, J. T. (1996) Design Challenges for Hemoproteins: The Solution Structure of Apocytochrome b_5, *Biochemistry 35*, 6519.
65. Englander, S. W., and Kallenbach, N. R. (1984) Hydrogen Exchange and Structural Dynamics of Proteins and Nucleic Acids, *Q. Rev. Biophys. 16*, 521−655.
66. Roder, H., Wagner, G., and Wütrich, K. (1985) Amide Proton Exchange in Proteins by EX1 Kinetics: Studies of the Basic Pancreatic Trypsin Inhibitor at Variable pH and Temperaure, *Biochemistry 24*, 7396−7407.
67. Yan, S., Kennedy, S. D., and Shohei, K. (2002) Thermodynamic and Kinetic Exploration of the Energy Landscape of *Borrelia burgdorferi* OspA by Native-state Hydrogen Exchange, *J. Mol. Biol. 323*, 363−375.
68. Mukhopadhyay, K., and Lecomte, J. T. J. (2004) A Relationship between Heme Binding and Protein Stability in Cytochrome b_5, *Biochemistry 43*, 12227−12236.
69. Ihara, M., Takahashi, S., Ishimori, K., and Morishima, I. (2000) Functions of Fluctuation in the Heme-Binding Loops of Cytochrome b_5 Revealed in the Process of Heme Incorporation, *Biochemistry 39*, 5961−5970.
70. Falzone, J. C., Wang, Y., Vu, B. C., Scott, N. L., Bhattacharya, S., and Lecomte, J. T. J. (2001) Structural and Dynamic Perturbations Induced by Heme Binding in Cytochrome b_5, *Biochemistry 40*, 4879−4891.
71. Kennedy, M. L., Silchenko, S., Houndonougbo, N., Gibney, B. R., Dutton, P. L., Rodgers, K. R., and Benson, D. R. (2001) Model Hemoprotein Reduction Potentials: The Effect of Histidine-to-Iron Coordination Equilibrium, *J. Am. Chem. Soc. 123*, 4635−4636.
72. Liu, D., Williamson, D. A., Kennedy, M. L., Williams, T. D., Morton, M. M., and Benson, D. R. (1999) Aromatic Side Chain-Porphyrin Interactions in Designed Hemoproteins, *J. Am. Chem. Soc. 121*, 11798−11812.

BI050564L